Moment Invariants for the Analysis of 2D Flow Fields

Michael Schlemmer, *Student Member, IEEE*, Manuel Heringer, Florian Morr, Ingrid Hotz, Martin-Hering Bertram,
Christoph Garth, Wolfgang Kollmann, Bernd Hamann, *Member, IEEE*, and Hans Hagen, *Member, IEEE*

Abstract—We present a novel approach for analyzing two-dimensional (2D) flow field data based on the idea of *invariant moments*. Moment invariants have traditionally been used in computer vision applications, and we have adapted them for the purpose of interactive exploration of flow field data. The new class of moment invariants we have developed allows us to extract and visualize 2D flow patterns, invariant under translation, scaling, and rotation. With our approach one can study arbitrary flow patterns by searching a given 2D flow data set for any type of pattern as specified by a user. Further, our approach supports the computation of moments at multiple scales, facilitating fast pattern extraction and recognition. This can be done for critical point classification, but also for patterns with greater complexity. This multi-scale moment representation is also valuable for the comparative visualization of flow field data. The specific novel contributions of the work presented are the mathematical derivation of the new class of moment invariants, their analysis regarding critical point features, the efficient computation of a novel feature space representation, and based upon this the development of a fast pattern recognition algorithm for complex flow structures.

Index Terms—Flow Visualization, Feature Detection, Pattern Extraction, Pattern Recognition, Image Processing.

---

1 INTRODUCTION

Feature extraction has become an enabling technology for interactive and visual data exploration. Especially highly complex scientific data sets like those generated by modern computational fluid dynamics simulations require us to develop more effective feature-based visualization approaches. A core effort for feature-based methods is the proper detection and classification of relevant information. But the classification of relevant information is not trivial. Many existing methods concentrate on the topological properties of a vector field. Though this is a reasonable and widely accepted methodology, most methods are very limited. For application, it is also interesting to extract and visualize more complex features, e.g., for the comparison of data sets. There is still a lack of methods that offer the recognition of freely defined user patterns in an acceptable amount of time. Complex pattern structures can with currently existing methods be recognized in just one configuration. For finding all occurrences in a data set, the pattern has to be computed multiple times in various scales and for each scale in various rotation angles. Since this is the bottle-neck of existing methods, there is the lack of a pattern description that is invariant to scaling and rotation operations. As a first step towards the goal of a real-time pattern detection algorithm for general flow fields, we present an approach for a rotation- and scale-invariant representation for 2D flow field patterns.

- *Michael Schlemmer, Manuel Heringer, Florian Morr, and Hans Hagen are with the University of Kaiserslautern, Germany*
  E-mail: schlemmer@informatik.uni-kl.de.
- *Martin Hering-Bertram is with the Fraunhofer Institut für Techno- und Wirtschaftsmathematik (ITWM) in Kaiserslautern, Germany.*
- *Ingrid Hotz is with the Konrad-Zuse-Zentrum für Informationstechnik Berlin (ZIB), FU Berlin, Germany.*
- *Christoph Garth is with the University of Kaiserslautern, Germany, and the Institute for Data Analysis and Visualization at the University of California, Davis, CA.*
- *Wolfgang Kollmann is with the Department of Mechanical and Aeronautical Engineering, University of California, Davis, CA.*
- *Bernd Hamann is with the Institute for Data Analysis and Visualization and Department of Computer Science, University of California, Davis, CA.*
- *All authors are affiliated with the International Research Training Group "Visualization of Large and Unstructured Data Sets" (IRTG 1131) of the German Research Foundation (DFG).*

We present a novel mathematical approach that extends the so-called *moment invariants* to flow data. Moment invariants are very common in font recognition and image understanding. The extension to flow fields is not trivial, since flow vector data is spatially correlated so that a component-wise approach would not be appropriate. The fact that vectors of a pattern structure change their values upon rotation of the structure is described in Section 3.1.

Besides presenting the mathematical foundations we also analyze the behavior of our novel *flow vector moment invariants* for topologically interesting features. This enables us to propose a very simple algorithm for detection of sinks, sources, and rotations, even of deformed versions.

Our main goal and second major contribution is an algorithm that can indeed detect patterns of arbitrary complexity on a circular domain for 2D flow fields. Using a tolerance control we also enable users to find similar pattern structures. The algorithm uses the precomputed moment invariants containing all possible pattern configurations. As the computation of the moment invariants of one reference pattern is extremely fast, the additional usage of a look-up-table for the moment values contained in a field reduces the search space and thus enables a fast pattern recognition.

The pre-computed structure for this search algorithm, the so-called moment pyramid (see Section 5.4) is built by the application of a fast convolution implementation. For this reason, moment basis functions have been discretized to masks, see Section 5.2.

A general pattern recognition method like this is also applicable for comparative visualization purposes. By pre-defining certain patterns for example data sets can be visually compared. There is also the possibility of performing comparative visualization by browsing the feature space built up by our moment invariants.

The main advantage of our pattern recognition method compared to others aiming the same goal is that with our method, it is possible to provide a rich information base in a pre-computation step that enables pattern detection and classification a lot faster. Besides speed, another main focus is generality. With this work we are presenting a fundamental first step towards future development of a fast 3D pattern classification and visualization. The theory part of our work is presented in Section 3 (mathematical definition of the moment invariants) and Section 4 (their properties for prominent flow features). After the computational aspects in Section 5 we present specific applications, as core the novel fast pattern recognition algorithm, and the results we obtained in Section 6.

2 RELATED WORK

Higher-level and more qualitative means for effective processing and analyzing complex scientific data sets is becoming increasingly important. Especially in the context of analyzing and understanding

the increasingly large and complex data sets produced by contemporary supercomputer simulations of realistic flow field phenomena, methods for meaningful feature extraction and feature visualization are required. Computational fluid dynamics data sets have motivated our research presented here especially for large datasets. Much work has been done in the area of automatic detection of features such as shock waves, vortex cores, boundary layer separation and reattachment lines, flow topology, and boundary layer characteristics. What features are considered to be most important depends on the specific application. Given the large amount of research that has been done in these areas an exhaustive overview would go beyond the scope of this paper. For a more detailed overview over common flow visualization methods we refer to [17] and [8]. While these methods are very successful when looking for these specific features they are too specific to approach more general structures, which might not belong to one of these classes.

A more flexible way to approach a wider range of predefined features is using methods from signal and image processing for pattern recognition. Heiberg et al. [11] introduced a convolution operator for pattern recognition applied to vector field data defined over an underlying uniformly spaced mesh. Ebling and Scheuermann modified this approach based on Clifford algebra [4] and applied it also to non-uniform data [5]. These methods are based on filters that in general are neither scale- nor rotation-invariant. To find patterns of different size and orientation one has to perform the filtering multiple times using adjusted filter masks. To speed up the time-intensive convolution step, Ebling and Scheuermann introduced a vector Fourier transform based on Clifford algebra [6]. This reduces the filter operation to a multiplication in frequency domain. For the unstructured case Schlemmer et al. [19] generalized this approach to a non-uniform fast Clifford Fourier transform. Even though the fast Fourier transform (FFT) improves the efficiency, the algorithms are still far away from supporting real-time pattern recognition for arbitrary pattern scales and orientations.

In image processing the problem was tackled by introducing invariant moments, first proposed by Hu [12]. By now, they have become a standard method in image understanding and font recognition. Therefore, many scientists use these moments or their derivatives for a wide range of applications, e.g., Liao et al. [15] for Chinese character recognition and Terrillon et al. [21] for face tracking in virtual reality (VR) environments. Abu-Mostafa and Psaltis [1] revised Hu's theory of moment invariants by introducing complex moments that have been further improved by Flusser [9, 10].

The definition of our invariant moments is in analogy to the definition of a moment basis by Flusser. With our approach, we are able to create a look-up table for the information given in the flow field speeding up the process of pattern recognition substantially.

Our concept of invariant moments opens new possibilities to compare data in moment space. Traditional comparison techniques are image-based, where visualizations for each data set are generated separately and compared side-by-side. For scalar fields a quantitative comparison method on the data level has been proposed by Edelsbrunner et al. [7]. Sahasrabudhe et al. [18] defined metrics for comparing data in the spatial domain, which are usable for images and other data sets. Previous work on comparative visualization for flow fields includes the work of Pagendarm et al. [16] and Verma and Pang [22], which is based on the comparison of stream and vortex lines. Recently, Svakhine et al. [20] and Callahan et al. [3] have presented systems that support comparative visualization. The use of our approach, which is based on scale- and rotation-invariant moments, offers a very flexible pattern-based similarity computation.

3 DEFINITION OF MOMENT INVARIANTS FOR FLOWS

3.1 Problem Description and Motivation

A major contribution of our work is the definition and realization of invariant moments for feature-based analysis of flow fields. Our method supports the fast recognition of arbitrarily defined patterns in given flow vector data. With arbitrarily defined patterns we mean patterns on a circular domain with arbitrary content. There are interesting examples where recognizing freely defined flow patterns can be useful in practice. Our main motivation however is building a solid foundation towards an interactive 3D environment for analyzing structures in scalar, vector, and tensor data. This work represents a first step towards this goal. Although, a similar pattern recognition in flow fields might also be performed with related methods, like the method of Ebling and Scheuermann, we are able to do this with higher accuracy, much faster, also for large data sets.

Moment Invariants, a technique known from image understanding, can be used for pattern recognition in scalar data. In this section we introduce a new class of moment invariants describing 2D flow vector patterns being invariant under translation, scaling, and rotation.

Moment invariants capture essential information of a given field, containing most of the information in its lower order elements (similar to a Fourier representation). The main advantage of this technique is that the pattern information is stored in a form that is invariant to translation, scaling, and rotation.

When generalizing the invariant moments to flow fields it is not enough to consider each component separately as it would be possible for spatially uncorrelated vector-valued data, e.g., color images. The definition of rotation invariance of scalar moment invariants is not appropriate for flow fields. This problem is illustrated in an example shown in Figure 1. In the following paragraph the mathematical
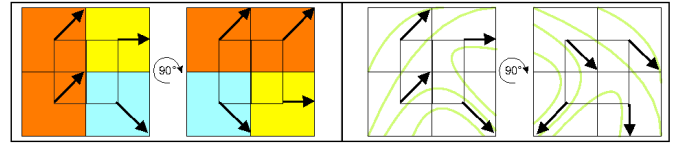

Fig. 1. Difference in the understanding of a rotation operation between spatially uncorrelated data (e.g., a vector representation of colors, (left part) and flow data (right part). While for uncorrelated data a rotation only applies to the domain, rotation of the (vector) values has to be taken into account for an invariant description of flow features.

foundations of our flow moment invariants are explained. Even though the physical meanings of moment invariants are an interesting research subject we will concentrate on their algebraic properties, since we consider those properties being most important for pattern recognition and visualization. As an example for application areas of moment invariants, Section 4 shows the characteristics of moment invariants for critical point features. For this special area, moment invariants are quite similar to other known descriptors like the Poincaré index. In contrast to the Poincaré index, moments are designed to handle more general patterns, not only critical point features.

3.2 Basics

Our derivation of flow vector moment invariants is based on complex moments, as used by Flusser [9]. We generalize the complex moments c'_{pq} to vector-valued functions. Let $f : \mathbb{R}^2 \to \mathbb{C} \cong \mathbb{R}^2$ be a map from $\mathbb{R}^2$ with $f \neq 0$ only in a compact subset $G \subseteq \mathbb{R}^2$. Let further $p, q \in \mathbb{N}$ and $i = \sqrt{-1} \in \mathbb{C}$. The complex moment of order $(p+q)$ of f is defined as

$$c'_{pq} = \int_{-\infty}^{\infty} \int_{-\infty}^{\infty} (x+iy)^p (x-iy)^q f(x,y) dx dy. \qquad (1)$$

Note, that we use the isomorphism of $\mathbb{R}^2$ and $\mathbb{C}$ to represent the image of f as complex values. By application of the binomial theorem complex moments of arbitrary order can be represented as linear combinations of regular moments:

$$c'_{pq} = \sum_{j=0}^{p} \sum_{k=0}^{q} \binom{p}{j} \binom{q}{k} (-1)^{q-k} i^{p+q-j-k} m_{j+k, p+q-j-k} \qquad (2)$$

with the regular moments

$$m_{pq} = \int\limits_{-\infty}^{\infty} \int\limits_{-\infty}^{\infty} x^p y^q f(x,y) dx dy. \tag{3}$$

3.3 Translation and Scale Invariance

In the scalar case translational invariance is obtained by shifting the original origin of function $f : \mathbb{R}^2 \to \mathbb{R}^2$ onto its centroid z_f^{scal}, being defined by $z_f^{scal} = (\bar{x}, \bar{y})^T = \left(\frac{m_{10}}{m_{00}}, \frac{m_{01}}{m_{00}} \right)^T$. As a similar function is likely to have a similar centroid, this method enables a translation-invariant comparison. In contrast to scalar fields, where the centroid corresponds to the center of mass, there is no obvious equivalent for vector-valued data. An appropriate definition of the centroid is strongly dependent on the specific application. Therefore we leave the centroid definition open in this section to keep the theory part of our work as general as possible. In practice, the centroid can be defined, for example, by vector length or by vector direction.

Scale invariance means that the moments do not change when the patterns are scaled. This can be achieved by scaling the moments appropriately. Again there are different possibilities to define scale invariance for vector fields. In particular we propose two definitions.

Let $f : G \to \mathbb{C}$ be a vector-valued function as defined above. Let further $\tilde{f} : \tilde{G} \to \mathbb{C}$ be a version of f scaled by a factor $s \in \mathbb{R} \backslash \{0\}$. The function f is scaled equally in domain and value: $\tilde{f}(x,y) = s \cdot f(\frac{x}{s}, \frac{y}{s})$. An invariant I_s with $I_s(f) = I_s(\tilde{f})$ is called *total scale invariant*.

This definition is very restrictive. Patterns are only recognized to be similar when both domain space and dependent vector field values scale in the same way. However, for many patterns it is more interesting to consider only the direction field. In these cases it would be advantageous to define scale invariance only on the domain, not on the image of f. A weaker definition appropriate for homogenized flow fields, is given in the following:

Let $f : G \to \mathbb{C}$ be a vector-valued function as defined above. Let further $\tilde{f} : \tilde{G} \to \mathbb{C}$ be a version of f, on a domain scaled by a factor $s \in \mathbb{R} \backslash \{0\}$: $\tilde{f}(x,y) = f(\frac{x}{s}, \frac{y}{s})$. An invariant I_s with $I_s(f) = I_s(\tilde{f})$ is called *domain scale invariant*.

These invariants can be obtained by multiplying the complex moments, as defined in Equation 1, with a scaling factor. For an invariant $I_s(f)$ this factor is defined by a power of the volume of the domain G of f. Combining translation and scale invariance, we can define scale- and translation-invariant complex moments as

$$c_{pq} = \frac{1}{v^\gamma} \int\limits_{-\infty}^{\infty} \int\limits_{-\infty}^{\infty} (\hat{x} + i\hat{y})^p (\hat{x} - i\hat{y})^q f(x,y) dx dy \tag{4}$$

with $v = \int_G 1 \, dx dy$, $\hat{x} = (x - \bar{x})$, $\hat{y} = (y - \bar{y})$, and $\gamma = \frac{p+q+3}{2}$ for total scale invariance, $\gamma = \frac{p+q+2}{2}$ for domain scale invariance. In analogy to equation (2), there is an alternative representation for c_{pq}:

$$c_{pq} = \sum_{j=0}^{p} \sum_{k=0}^{q} \binom{p}{j} \binom{q}{k} (-1)^{q-k} i^{p+q-j-k} \eta_{j+k,p+q-j-k} \tag{5}$$

with the normalized central moments

$$\eta_{pq} = \frac{1}{v^\gamma} \int\limits_{-\infty}^{\infty} \int\limits_{-\infty}^{\infty} \hat{x}^p \hat{y}^q f(x,y) dx dy. \tag{6}$$

3.4 Rotation Invariance

For the derivation of rotational invariance it is essential to rewrite the moments in polar form. This can be done similarly for regular complex

moments c'_{pq} as well as the translation and scale invariant version c_{pq}. Since the derivation of rotation invariance is independent of scale- and translation-invariance, we only use the term *complex moments* as it is more general. The substitutions of $\hat{x} = r\cos(\varphi)$ and $\hat{y} = r\sin(\varphi)$ yield

$$c_{pq} = \frac{1}{v^\gamma} \int\limits_{0}^{\infty} \int\limits_{0}^{2\pi} r^{p+q+1} e^{i(p-q)\varphi} f(r,\varphi) d\varphi dr. \tag{7}$$

Lemma 3.1 *Let $\tilde{f}$ be a version of f rotated around its centroid with angle α: $\tilde{f}(r,\varphi) = e^{i\alpha} \cdot f(r,\varphi - \alpha)$. Let $\tilde{c}_{pq}$ be a complex moment of order $(p+q)$ of $\tilde{f}$. Then:*

$$\tilde{c}_{pq} = e^{i(p-q+1)\alpha} c_{pq} \tag{8}$$

Proofs are given in the Appendix. Using this lemma, we can derive a set of moments that is invariant to rotations for 2D flow fields. For this purpose, the factor $e^{i(p-q+1)\alpha}$ has to be eliminated by an appropriate combination of complex moments c_{pq}.

Theorem 3.1 (Construction of rotation-invariant moments)
Let $c_{p_j q_j}$, $j = 1,...,n$, be complex moments of a map $f : G \to \mathbb{C} \cong \mathbb{R}^2$, with $G \subseteq \mathbb{R}^2$ and let $\sum_{j=1}^{n} (p_j - q_j) = -n$. Then

$$I_r = \prod_{j=1}^{n} c_{p_j q_j} \tag{9}$$

is invariant under rotation, i.e., I_r does not change when f is rotated with an arbitrary angle α.

3.5 Invariant Moment Basis for Flows

A combination of complex moments needs to satisfy the property $\sum_{j=1}^{n} (p_j - q_j) = -n$ as stated in Theorem 3.1 to form moment invariants. Using the shown methods to derive translation-, scale- and rotation-invariant moments, an infinite number of moment invariants can be generated. In practical applications, only a finite number can be used. In scalar application, moments are in general limited to order three, since higher-order moments become more and more numerically instable. Furthermore, almost all information is stored in lower-order moments. For our applications we have constructed a basis $\mathscr{B}$ of order two of invariant moments, according to theorem 3.1, incorporating the translation and scale invariance given in Section 3.3. A basis of moment invariants of a specific order n is a set of moments with order $\leq n$ that contains only independent moments and can represent completely all other moments of this order. For more details on the definition of a moment basis, we refer to Flusser [9]. Our basis for flow vector moment invariants is defined as follows:

$$\mathscr{B} = \left\{ c_{01}, c_{00}c_{02}, c_{11}c_{02}, c_{10}c_{02}^2, c_{20}c_{02}^3 \right\}. \tag{10}$$

As mentioned, those complex values describe a vector function invariantly under translation, scaling, and rotation. There is another very interesting property of those moments. The real part of the complex moments is invariant to mirror operations, while the imaginary part just changes its sign. This means that mirrored occurrences of a pattern structure can also be recognized by regarding the real part and the absolute value of the imaginary part. For patterns being self-symmetric the imaginary part is zero. For improved notation in the following sections, we define abbreviations for our complex-valued basis elements:

$$\begin{aligned}
\Psi_1 &= c_{01}, \\
\Psi_2 &= c_{00}c_{02}, \\
\Psi_3 &= c_{11}c_{02}, \\
\Psi_4 &= c_{10}c_{02}^2, \\
\Psi_5 &= c_{20}c_{02}^3.
\end{aligned} \tag{11}$$

In contrast to the scalar case, c_{00} is not rotation-invariant. This observation arises from the fact that not only the domain, but also the vector values change under rotation of the flow pattern (see Figure 1).

homogeneous flow	source / divergence	sink / convergence	counter-clockwise rotation	clockwise rotation	compressed rotation	saddle
$\Psi_1 = 0$ $\Psi_{2,3,4,5} = 0$	$\Psi_1 = \frac{2}{3\sqrt{\pi}}$ $\Psi_{2,3,4,5} = 0$	$\Psi_1 = -\frac{2}{3\sqrt{\pi}}$ $\Psi_{2,3,4,5} = 0$	$\Psi_1 = i\frac{2}{3\sqrt{\pi}}$ $\Psi_{2,3,4,5} = 0$	$\Psi_1 = -i\frac{2}{3\sqrt{\pi}}$ $\Psi_{2,3,4,5} = 0$	$\Psi_1 \approx -i0.1677$ $\Psi_{2,3,4,5} = 0$	$\Psi_1 = 0$ $\Psi_{2,3,4,5} = 0$

Fig. 2. Invariant moment values for proto-typical flow features. The fact that all second-order moments ($\Psi_{2,3,4,5}$) are zero for linear vector fields enables an easy recognition of these features.

4 VECTOR MOMENT CHARACTERISTICS FOR CRITICAL POINTS

In this paragraph we exemplarily provide some continuous moment representation for some proto-typical 2D critical points. This continuous evaluation is compared with our discrete computation results in Section 6.2. Critical points are only a special class of patterns we want to observe with our method. However, we consider them as a good example to show how the moments are evaluated continuously and provide some information on their behavior.

As an example for a pattern we present the continuous values of our vector moment invariants for a counter-clockwise rotation. It can be described continuously by $f : G \to \mathbb{R}^2$:

$$f(x,y) = \begin{cases} (0,0)^T & \text{, if } x = y = 0 \\ \frac{1}{\sqrt{x^2+y^2}} \begin{pmatrix} -y \\ x \end{pmatrix} & \text{, otherwise} \end{cases} \quad (12)$$

The moments of f over a circular domain with radius one and center in the critical point can be derived with equation (3):

$$m_{pq} = \int_{-1}^{1} \int_{-\sqrt{1-x^2}}^{\sqrt{1-x^2}} x^p y^q \frac{-y + i x}{\sqrt{x^2+y^2}} dy dx \quad (13)$$

for $(p+q) \leq 2$ yielding

$$\begin{aligned} m_{01} &= -\tfrac{1}{3}\pi & m_{10} &= i\tfrac{1}{3}\pi \\ m_{00} &= m_{02} = m_{11} = m_{20} = 0. \end{aligned} \quad (14)$$

As we integrate over the unit circle (having area π) with the critical point as centroid, it yields $\eta_{pq} = \frac{1}{\pi^\gamma} m_{pq}$, $\gamma = \frac{p+q+2}{2}$. Therefore, we can apply equation (5) and (11) to calculate our moment invariants:

$$\begin{aligned} \Psi_1 &= i\frac{2}{3\sqrt{\pi}} \approx 0,376126389\,i \\ \Psi_2 &= \Psi_3 = \Psi_4 = \Psi_5 = 0. \end{aligned} \quad (15)$$

This calculation can also be performed for other critical features, i.e., clockwise rotation, convergence, divergence, or saddles. For these critical features we also obtain interesting results as shown in Figure 2. Obviously, only the first-order invariant moment $\Psi_1 = c_{01}$ is non-zero for most of the observed features. Rotation patterns have a purely imaginary value in c_{01}, while it is real for convergence and divergence. This fact even holds for compressed versions offering a simple algorithmic way for a good classification of these features. Furthermore, turning each single vector belonging to a pattern $90°$ counter-clockwise yields a multiplication of c_{01} with the complex number i. Moreover, this fact holds for any kind of pattern.

We discovered that the continuous representation of purely homogeneous flow as well as saddles have their moment invariants being zero. This can be resolved by taking into account an already precomputed parameter: the absolute value of the sum over all vectors in the pattern $|m_{00}|$. For saddles $|m_{00}|$ vanishes, while it is definitely non-zero for a homogeneous flow. Instead of $|m_{00}|$ one can also use the shifted and scaled version $|c_{00}|$. We present a method for highlighting critical features using the properties described in Section 6.2 and as second-order moment invariants are relevant for more complex patterns, we also present a pattern recognition algorithm suitable for search patterns of arbitrary complexity on a circular domain.

5 COMPUTATION OF MOMENT INVARIANTS FOR FLOWS

5.1 Basic Considerations

Invariant moments are mainly used in image processing and font recognition. They are usually applied to a pre-segmented portion of a given data set. A vector field segmentation implies, however, strong restrictions to special regions of flow behavior. To keep the system general for the recognition of arbitrary flow patterns, the whole data set has to be taken into account. Thus, we developed a multi-scale approach for analyzing 2D flow data, described in Section 5.4. This approach can be used for an invariant pattern recognition. To extract the information of a data set at various scales, one has to use filter functions to extract the information. For covering the whole field one can apply a correlation operation. Thus, we discretize the flow vector moments to filter masks and perform the correlation by a convolution of mirrored masks with the field enhanced by a Fast Fourier Transform (FFT) implementation. The discretization and convolution process is described in detail in Section 5.2.

The convolution is computed for all discrete radii resulting in the moment pyramid. Since the convolution operation increases continuity by one degree, small perturbations in the radii between these discrete positions tend to have only very limited effects. Since the convolution operator covers the whole field, translation invariance becomes obsolete for this special application of the theory. This does not mean it becomes obsolete in general, i.e., for our setting we have to choose the centroid to be located in the center of each filter mask.

We have mentioned two types of scale invariance in Section 3. Depending on the application, one might be only interested in the directional behavior of vector patterns. If total scale-invariant moments are chosen, vector magnitude has a big influence on the results, i.e., patterns that are equal in directions and different in scale are not recognized. Therefore, we decided to homogenize the vector length of the field and store the magnitude information separately as a scalar field. The direction information can be examined using our flow vector moments with domain scale invariance. Flow magnitude can be regarded as an image and be processed using our pyramid approach with the standard scalar moment invariants. If one is only interested in recognizing structures that are both, similar in vector direction and length, one has to change the computation from *domain scale invariance* to *total scale invariance*.

5.2 Correlation with Moment Filter Masks

For an efficient computation of the vector moments of the complete field we have implemented a correlation of the field with specific moment filter masks. In equation (5) we have shown how complex mo-

ments can be represented by normalized central moments. Those moments can be easily derived from regular moments m_{ij}. Regular moment filter masks can be discretized and computed independent from the data. It is the correlation of these masks with f that result in the moments m_{ij}. For an efficient computation, we perform the correlation as a convolution with mirrored filter masks. The convolution can be enhanced by using component-wise Fast Fourier Transforms (FFT) and multiplication in frequency domain. The normalized central moments η_{ij} are calculated by application of shifting and scaling onto m_{ij}. As rotation invariance cannot be fully guaranteed for rectangular masks, the moments are trimmed to a circular isotropic domain around the chosen centroid. Those can be used to compute our complex moments c_{pq} (see equation (5)). Inserting these values into our invariant basis, we obtain according to equation (11) the values $\Psi_1, \ldots, \Psi_5$. These values are finally invariant to translation, scaling, and rotation for any kind of given pattern.

5.3 Overcoming Discretization Issues

For small mask sizes the coarse discretization of the moment calculation introduces a high relative error. This is because the domain ought to be circular. Larger mask sizes are better in approximating this circle. So, using super-sampling we can strongly increase accuracy for smaller mask sizes. The heuristic we applied for our data is to use a five times super-sampled field for mask sizes from 5x5 to 20x20, and for all others the regular field size. This procedure lifts accuracy of a 5x5 moment computation to the stable 21x21 moment computation. The improvement in accuracy is also depicted in Table 1 of our results section. The fact that an improvement can be reached by super-sampling, as well as the fact that our theoretic foundations are based on continuous data also show that our method is, though not implemented yet, also applicable on arbitrary grids or pure point set data without an underlying grid (see also Section 5.5).

5.4 Multi-scale Moment Pyramid

For each scale of the filter masks correlations are performed, each resulting in a field on a two-dimensional domain containing the invariant moments $\Psi_1, \ldots, \Psi_5$. Those fields become smaller for increasing scale of the filter masks, since we decided to omit the border in our implementation. Thus, the resulting collection of moment fields is called *moment pyramid*.

A moment pyramid provides a discretized description of all possible vector patterns of an underlying field, stored with height corresponding to the scale of the pattern and the corresponding position at each specific scale level of the pyramid.

5.5 Generalization

Although our implementation concentrates on circular features, there are ways to handle differently shaped patterns. Patterns can be subdivided into (overlapping) circular regions. Those regions can be analyzed or used as input for a search algorithm. A search algorithm regarding these connected regions has to be extended with a method that compares the positions of each circular pattern finding, enabling a classification of non-circular patterns. Although, global features, like for example separatrices cannot be found directly with this method one might specify pattern regions that are characterizing separatrices. Moment invariants might be utilized for vector field segmentation also resulting in separatrices in future work.

Another point that has already been mentioned is the extension to unstructured grids. This can be done in an elegant fashion, as the theory of vector moment invariants is formulated for continuous data. Though, to achieve this there is a need for a new data structure, as the presented moment pyramid has been designed for uniformly structured data. Another possibility would be to keep the data structure for this purpose and just use our super-sampling method at very high resolution for unstructured grid data. Of course, in this case a good interpolation method is essential for good results. An additional uncertainty visualization should also be included in this case, depending on the density of the input samples. This can also be an aspect of future development.

6 APPLICATIONS AND RESULTS

6.1 Analyzed Data

In this section we describe two data sets from CFD: a simulation of a turbulent swirling jet flow with low Reynolds number and the Boussinesq Flow, both based on the solution of Navier-Stokes equations.

6.1.1 Low Re-number turbulent swirling jet flow

The development of a recirculation zone in a swirling flow is investigated by numerical simulation. This type of flow is relevant to several applications where residence time is important to enable mixing and chemical reactions.

The unsteady flow in a swirling jet is simulated with a hybrid spectral - finite difference method. The Navier-Stokes equations for an incompressible, Newtonian fluid are set up in cylindrical coordinates in terms of (complex-valued) stream-function and pressure modes, which are governed by Helmholtz PDEs, and azimuthal velocity and vorticity modes, which are determined by evolution PDEs.

All equations are dimensionless containing the Reynolds number $Re \equiv \frac{v_z(0,z_0)D}{v}$ and the swirl number as defined by Billant et al. [2]: $S \equiv \frac{2v_\theta(R/2,z_0)}{v_z(0,z_0)}$, where $z_0 = 0.4D$, $D = 2R$ is the nozzle diameter and v the kinematic viscosity.

The PDEs for the Fourier modes are discretized in the meridional plane with 8th order central difference operators for the non-convective terms and with a 9th order, upwind-biased operator [14] for the convective terms. Time integration is accomplished with an explicit s-stage, state space Runge-Kutta method ([23], [13]) where the Helmholtz PDEs for the stream-function and pressure modes are solved at each stage, the present method is fourth order accurate with $s = 5$. The time step is controlled by the minimum of two criteria: The limit set by linearized stability analysis and the limit set by the error norms of an embedded third order Runge-Kutta scheme [23]. The Helmholtz PDEs for stream-function and pressure modes are solved with an iterative method using deferred corrections and LU-decomposition of the coefficient matrices. The deferred corrections method is designed to reduce the bandwidth of the coefficient matrices. It converges rapidly using about ten to twenty steps, the rate of convergence increasing with the azimuthal wavenumber.

The simulation used for our feature-based analysis in section 6.3 results for the Reynolds number $Re = 900$ and the swirl number $S = 1.41$ within the range of the experiments of Billant et al. [2] at a time ($t = 12.4$) when the recirculation bubble has formed and the initial symmetries of the flow field have been broken due to the disturbances introduced at the entrance boundary.

6.1.2 Boussinesq Flow

The second investigated data set is a classical Boussinesq approximation to simulate the flow generated by a heated cylinder. This approximation adds a source term proportional to the temperature (modeled as a diffusive material property) to the vertical component of the velocity field. The cylinder serves as a temperature source and thereby generates a plume of upward flowing material. As the plume moves upward, its outer layers exchange heat with the surrounding flow, resulting in inhomogeneous friction and hence turbulent flow.

6.2 Visualization of Critical Points

As shown in Section 4, invariant moments have certain properties for critical point features. We propose an algorithm for highlighting 2D critical point features, i.e., rotations, sinks, sources. Saddles need further inspection, as first and second-order moment invariants are zero, equally to any homogeneous flow pattern. This can be solved as explained in section 4 by observing the value of $|m_{00}|$ or $|c_{00}|$.

Our algorithm uses a pre-processing step to compute a sorted list of pyramid positions. The positions are sorted according to a combination of the absolute values of the second-order moments $\Psi_{2,3,4,5}$, i.e., sorted according to a parameter $n = |\Psi_2| + |\Psi_3| + |\Psi_4| + |\Psi_5|$. The resulting list has the critical features, as well as homogeneous flow

resolution	$\mathrm{Im}(\Psi_1)$	absolute deviation	relative deviation [%]
5×5	0.408543	0.032417	8.6187
$5 \times 5^*$	0.380274	0.004148	1.1028
10×10	0.386398	0.010272	2.7311
$10 \times 10^*$	0.376822	0.000695	0.1849
25×25	0.373890	0.002236	0.5945
50×50	0.379709	0.003582	0.9524
75×75	0.376525	0.000398	0.1059
100×100	0.376557	0.000430	0.1144
200×200	0.376339	0.000213	0.0567
continuous	0.376126	-	-

Table 1. Results of the discrete moment computations compared with the continuous value of a counter-clockwise rotation feature (*using the super-sampling approach). Super-sampling improves accuracy. Values converge faster for odd pattern sizes. For proper recognition of exact patterns the relative deviation parameter δ should be chosen by assuming worst case deviation of the calculation, i.e., to capture small scales $\delta \approx 1\%$, and higher for the recognition of similar patterns.

S-shaped pattern	Diverging pattern
$\Psi_1 = 9.804 \cdot 10^{-03} - i \cdot 2.294 \cdot 10^{-01}$	$\Psi_1 = 1.064 \cdot 10^{-01} + i \cdot 8.634 \cdot 10^{-03}$
$\Psi_2 = -2.294 \cdot 10^{-01} - i \cdot 8.264 \cdot 10^{-03}$	$\Psi_2 = 1.581 \cdot 10^{-02} + i \cdot 1.543 \cdot 10^{-03}$
$\Psi_3 = -1.888 \cdot 10^{-03} + i \cdot 1.187 \cdot 10^{-03}$	$\Psi_3 = 2.445 \cdot 10^{-03} + i \cdot 2.285 \cdot 10^{-04}$
$\Psi_4 = -1.894 \cdot 10^{-04} + i \cdot 5.633 \cdot 10^{-06}$	$\Psi_4 = -3.709 \cdot 10^{-05} - i \cdot 4.484 \cdot 10^{-06}$
$\Psi_5 = -2.226 \cdot 10^{-07} - i \cdot 1.540 \cdot 10^{-06}$	$\Psi_5 = -2.367 \cdot 10^{-09} - i \cdot 6.079 \cdot 10^{-09}$

Table 2. Moment invariants for two example search patterns. An S-shaped structure from the swirling jet data set (see Figure 4) and a diverging structure in the Boussinesq flow data (see Figure 5).

patterns, at its front end. Excluding all feature values with the first-order value Ψ_1 near or equal to zero, results in a list that is sorted according to criticality. Processing this list is straightforward: the list is traversed to a user-defined point. Each entry contains the pyramid position that maps directly to position and scale in the field, enabling a fast visualization. We used this method to highlight rotations in a Boussinesq flow data set (see Figure 3).

Operating on discretized features we obtain approximations of the continuous values. Discretization results and deviations are presented in Table 1 exemplarily for the rotation pattern observed in section 4. As one can see, our super-sampling approach for small scales strongly helps improving the results obtained with the moment invariants.
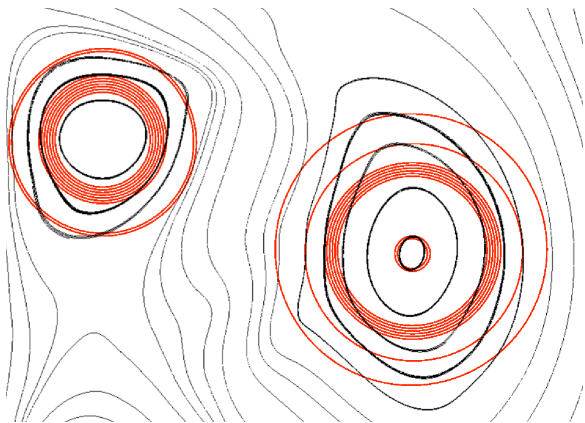

Fig. 3. Rotations in a Boussinesq flow (see Section 6.1.2). Features found by searching with the criticality index being highlighted by red colored circular region markers.

6.3 Fast Pattern Recognition in Flow Fields

Besides the recognition of critical points, moment invariants can be used for the fast recognition and classification of arbitrary features. We implemented a fast pattern recognition for 2D flow vector data using the theory of our flow vector invariants. In a pre-processing step a moment pyramid is computed for the given data. This pyramid stores the complex moment invariants $\Psi_1 \ldots \Psi_5$ for local regions of the field. We further compute a sorted offset of the moment values of Ψ_1 linking to the positions in our pyramid. We have chosen Ψ_1, as it is a first-order component containing the major part of the information. The pattern matching algorithm can now be performed very efficiently. A pattern

is selected, the computation of the invariant moments for a single pattern is done rapidly, a delta region around the computed offset reveals a short list of similar pattern candidates, which can be compared in the remaining moment invariants $\Psi_2 \ldots \Psi_5$.

As arbitrary patterns are recognized invariant to scale and rotation, no time-intensive additional convolutions are necessary during execution time. Similar patterns can be highlighted almost in real-time. The only drawback of this method, the high usage of memory, could be overcome by storing only the first component in the pyramid. This would save disk space, but on the other hand lead to a little higher latency, as moments must be computed for all matches. Since we use the complete moment pyramid also for other applications, we decided to perform our pattern recognition with the larger version.

In contrast to other algorithms for pattern recognition in vector fields (like Ebling and Scheuermann [4] or Heiberg [11]), our algorithm is able to detect any kind of pattern without an extra computation of rotated or scaled versions. To illustrate this, we discuss two examples for extra-ordinary pattern searches, showing that the patterns do not have to satisfy any special properties. Figure 4 shows the swirling jet data set discussed in Section 6.1.1, the pattern, and the matches. The moment invariants for the search pattern can be found in Table 2. Each pattern has been detected correctly. Note that there might be other S-shaped structures not being found because of their different directional behavior not being depicted in the streamline representation. This can be tackled by comparison of the magnitude of real and imaginary part in the first-order component Ψ_1 separately so that the sign is skipped. The Boussinesq flow, explained in Section 6.1.2, is shown in Figure 5. We searched for a specific diverging flow pattern, and obtained good results. By increasing the relative deviation δ, the search space is increased. This takes effect on computation time, but increases the number of matches. We integrated these algorithms into our CoVE (Comparative Visualization Environment) system enabling a parallel pattern search in multiple data sets. Patterns can be specified by selection, by definition (through an integrated pattern editor), or by browsing through invariant moment space. The identified patterns are then highlighted in all visualized data sets, allowing us to compare in a highly effective way complex flow data sets based on arbitrary flow features. Comparing the algorithm to the algorithms of Heiberg [11], and Ebling and Scheuermann [4], our pre-processing step for all searches is approximately as expensive as the other methods to search for one single pattern. The result of our pre-processing however, makes it possible to search for all kinds of patterns in almost real time, even for larger data sets. We now explain, why our pre-processing step and the search times of the mentioned methods are similar. While for the other algorithms, many rotated versions for any scale of the pattern have to be correlated with the chosen field, we perform a correlation with ten pre-defined basis functions m_{ij}. This correlation step is the most expensive (but still highly optimized) part and has to be performed for all methods. For our method, we need to sort and store the results as our search data basis, while the other methods do not need to do this. The other methods have to compute the rotated and scaled versions prior to the correlation and they have to combine the search results for the rotated and scaled versions to a final similarity map. All in all our pre-processing step and the mentioned algorithms got approximately the same complexity. Having the pre-processing step done once, multiple freely definable patterns can be searched for each in almost real
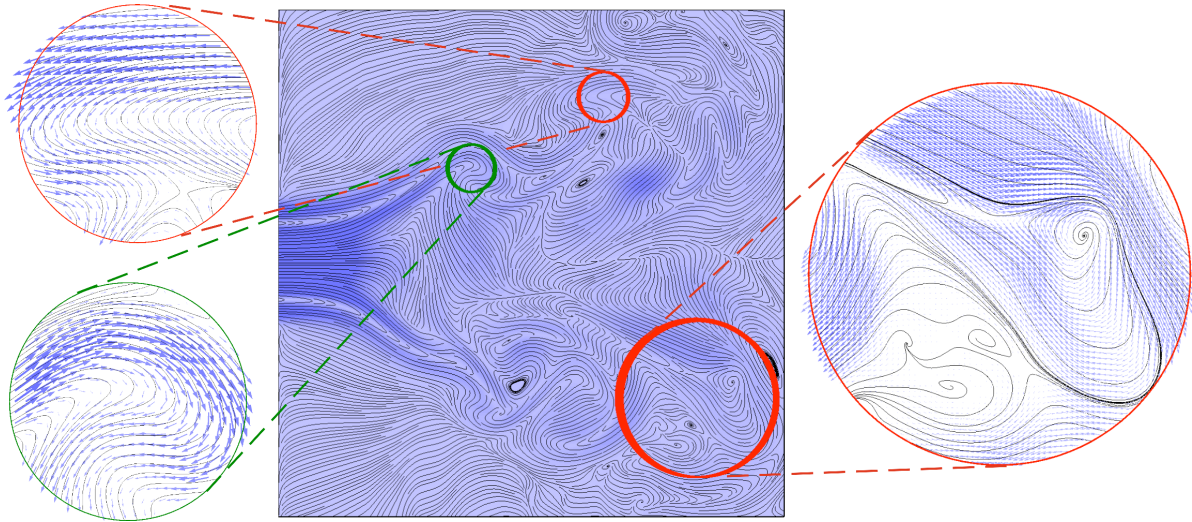
Fig. 4. Swirling jet flow (Section 6.1.1). We search for an S-shaped pattern (green circle) and find it three times at different scales for $\delta = 0.7$ (green and red circles). General data is visualized with streamlines, close-ups of the matching structures include a hedgehog representation. Even though the swirls in the right image distract the viewers attention the global S-shaped structure has been recognized. Underlying color map and colors of the hedgehog representation of the zoomed versions display the velocity of the swirling jet data.
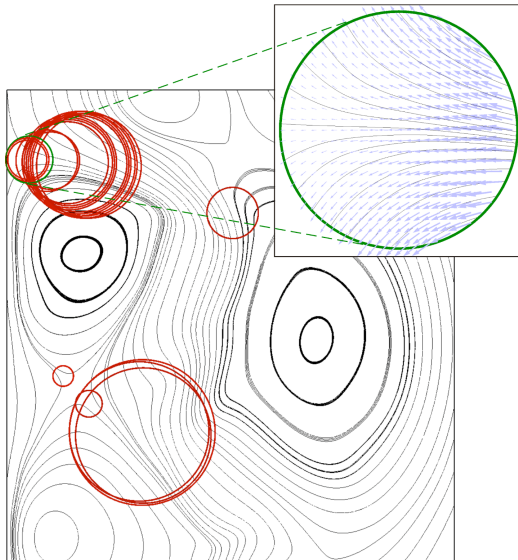
Fig. 5. Search results (red) for a specific pattern in the Boussinesq flow with $\delta = 0.5$. The original pattern is highlighted by a green circle and a zoomed representation is given in the upper right corner.
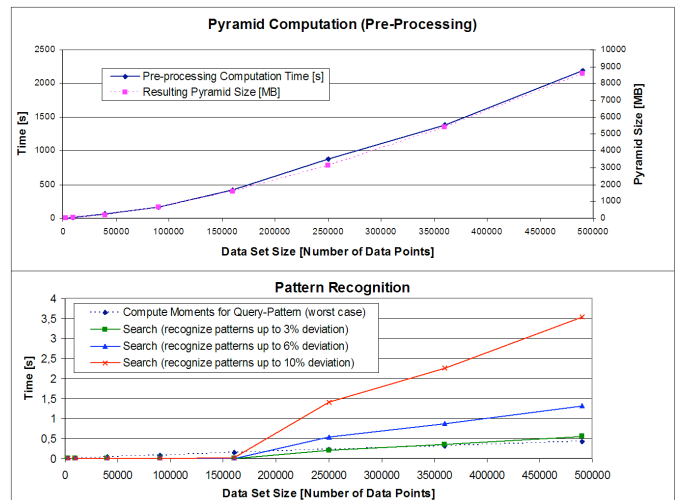

Fig. 6. Computation results for scaled versions of the Boussinesq data set. The upper diagram shows information on the pre-processing step for generating the moment pyramid. The lower diagram shows the recognition times for arbitrary circular patterns. A sudden time increase at a data set size of 500x500 can be observed for the reason that for larger data sets the pyramid exceeds the main memory. Search times still remain acceptable.

time. This is far better than the computation time for one single pattern using the other algorithms. The only disadvantage of the new method is that these patterns have to be defined on a circular domain. This issue can be overcome by an advanced search approach as discussed in Section 5.5. Quantitative results for our pre-processing step, the calculation of the moment pyramid and for the search operations are illustrated in Figure 6. Results have been computed on a Athlon X2 4600+ with 2GB RAM. The point where search times suddenly increase can be explained by the fact that for larger data sets the search in the moment pyramid has to be performed on the hard disk and not in the main memory. The higher we chose the deviation, the less similar the result patterns become. If one would like to find somewhat similar patterns, he or she can enter a higher deviation. This is more expensive as more possible results have to be compared with the actual moment values. A smaller deviation is a more strict criterion and yields less result positions, meaning less computation time.

7 CONCLUSIONS

We have presented a new class of moment invariants. Our first contribution presented here is the mathematical derivation of these invariants. They are able to provide a representation of correlated vector data, i.e., flow data, being invariant to translation, scaling and rotation. We further researched their properties and found that moment invariants also serve as a good classifier for flow data, even when only using moments of lower order. Finally, we have presented two algorithms for fast recognition of flow patterns. One algorithm utilizes the fact that for linear flow fields second-order moments are zero to recognize critical points. Our second and even more important contribution to the state of the art of interactive visual data exploration is a new algorithm that uses a pre-processing step to compute the moment invariants and

an indexing system that enables fast recognition of pattern structures of arbitrary content (defined on circular domains). This pattern search can be performed on many datasets in parallel, enabling comparative visualization for self-defined or chosen patterns. Invariant moments are capable of being applied to arbitrary grid structures, as their definition is continuous. Future work will focus on defining orthogonal moment invariants for flow fields, the practical implementation of moments derived from pure point data without underlying grid structure, research on time-dependent 2D flow fields, segmentation of flow fields using these invariants, and the mathematical theory for moment invariants for flow fields defined on 3D spatial domains. The latter might be achieved by the usage of a quaternion basis or by modification of other scalar algebraic invariant moment formulations.

ACKNOWLEDGEMENTS

REFERENCES

[1] Y. S. Abu-Mostafa and D. Psaltis. Recognitive aspects of moment invariants. *IEEE Transactions on Pattern Analysis and Machine Intelligence*, 6(6):698–706, November 1984.

[2] P. Billant, J.-M. Chomaz, and P. Huerre. Experimental study of vortex breakdown in swirling jets. *Journal of Fluid Mechanics*, 376:183–219, Dec. 1998.

[3] S. P. Callahan, J. Freire, E. Santos, C. E. Scheidegger, C. T. Silva, and H. T. Vo. Vistrails: Visualization meets data management. In *ACM SIGMOD*, pages 745–747, 2006.

[4] J. Ebling and G. Scheuermann. Clifford convolution and pattern matching on vector fields. In *Proceedings of IEEE Visualization 2003*, pages 193–200, 2003.

[5] J. Ebling and G. Scheuermann. Clifford convolution and pattern matching on irregular grids. In *Scientific Visualization: The Visual Extraction of Knowledge from Data*. Springer-Verlag, 2005.

[6] J. Ebling and G. Scheuermann. Clifford Fourier transform on vector fields. *IEEE Trans. Vis. Comput. Graph.*, 11(4):469–479, 2005.

[7] H. Edelsbrunner, J. Harer, V. Natarajan, and V. Pascucci. Local and global comparison of continuous functions. In *IEEE Visualization*, pages 275–280, 2004.

[8] G. Erlebacher, C. Garth, R. S. Laramee, H. Theisel, X. Tricoche, T. Weinkauf, and D. Weiskopf. Texture and feature-based flow visualization - methodology and application. In *IEEE Visualization 06 Tutorial*, 2006.

[9] J. Flusser. On the independence of rotation moment invariants. *Pattern Recognition*, 33(9):1405–1410, 2000.

[10] J. Flusser and T. Suk. Pattern recognition by affine moment invariants. *Pattern Recognition*, 26(1):167–174, January 1993.

[11] E. Heiberg, T. Ebbers, L. Wigström, and M. Karlsson. Three-dimensional flow characterization using vector pattern matching. *IEEE Trans. Vis. Comput. Graph.*, 9(3):313–319, 2003.

[12] M.-K. Hu. Visual pattern recognition by moment invariants. *IRE Transactions on Information Theory*, 8(2):179–187, February 1962.

[13] C. A. Kennedy, M. H. Carpenter, and R. M. Lewis. Low-storage, explicit runge-kutta schemes for the compressible navier-stokes equations. *Appl. Numer. Math.*, 35(3):177–219, 2000.

[14] Y. Li. Wavenumber-extended high-order upwind-biased finite-difference schemes for convective scalar transport. *J. Comput. Phys.*, 133(2):235–255, 1997.

[15] S. Liao, Q. Lu, and K. Lee. Recognition of chinese characters by moment feature extraction. In *International Conference on Computer Processing of Oriental Languages*, pages 566–571, 1997.

[16] H.-G. Pagendarm and B. Walter. Competent, compact, comparative visualization of a vortical flow field. *IEEE Transactions on Visualization and Computer Graphics*, 1(2):142–150, 1995.

[17] F. Post, B. Vrolijk, H. Hauser, R. Laramee, and H. Doleisch. Feature extraction and visualization of flow fields. In *In Eurographics 2002 State of the Art Reports*, pages 69–100. The Eurographics Association, Saarbrücken, Germany, 2002.

[18] N. Sahasrabudhe, J. E. West, R. Machiraju, and M. Janus. Structured spatial domain image and data comparison metrics. In *VIS '99: Proceedings of the conference on Visualization '99*, pages 97–104, Los Alamitos, CA, USA, 1999. IEEE Computer Society Press.

[19] M. Schlemmer, I. Hotz, V. Natarajan, B. Hamann, and H. Hagen. Fast clifford fourier transformation for unstructured vector field data. In *Proc. Intl. Conf. Numerical Grid Generation in Computational Field Simulations*, pages 101–110, 2005.

[20] N. Svakhine, Y. Jang, D. S. Ebert, and K. P. Gaither. Illustration and Photography Inspired Visualization of Flows and Volumes. In *IEEE Visualization 2005*, 2005.

[21] J. C. Terrillon, M. David, and S. Akamatsu. Automatic detection of human faces in natural scene images by use of a skin color model and of invariant moments. In *FG '98: Proceedings of the 3rd. International Conference on Face & Gesture Recognition*, page 112, Washington, DC, USA, 1998. IEEE Computer Society.

[22] V. Verma and A. Pang. Comparative flow visualization. *IEEE Transactions on Visualization and Computer Graphics*, 10(6):609–624, 2004.

[23] R. Winkler. Stochastic differential algebraic equations of index 1 and applications in circuit simulation. *J. Comput. Appl. Math.*, 163(2):435–463, 2004.

APPENDIX

Proof of Lemma 3.1:

Using the substitution $\Phi(r,\varphi) = \begin{pmatrix} r \\ \varphi - \alpha \end{pmatrix}$ we obtain:

$$c_{pq} = \frac{1}{v^\gamma} \int_0^\infty \int_0^{2\pi} r^{p+q+1} e^{i(p-q)\varphi} f(r,\varphi) d\varphi dr$$

$$\stackrel{\Phi}{=} \frac{1}{v^\gamma} \int_0^\infty \int_\alpha^{2\pi+\alpha} r^{p+q+1} e^{i(p-q)(\varphi-\alpha)} f(r,\varphi-\alpha) d\varphi dr$$

$$= e^{-i(p-q+1)\alpha} \underbrace{\frac{1}{v^\gamma} \int_0^\infty \int_0^{2\pi} r^{p+q+1} e^{i(p-q)\varphi} \tilde{f}(r,\varphi) d\varphi dr}_{\tilde{c}_{pq}}$$

$$= e^{-i(p-q+1)\alpha} \tilde{c}_{pq}$$

$\square$

Proof of Theorem 3.1:

Let $\tilde{f}$ be a rotated version of f (counter-clockwise around the origin), i.e., $\tilde{f}(r,\varphi) = f(r,\varphi-\alpha)$ where α is the angle of rotation. Further let the complex moment of the order $(p+q)$ of $\tilde{f}$ be denoted as $\tilde{c}_{pq}$. One can derive the following:

$$\sum_{j=1}^n (p_j - q_j) = -n \qquad \Leftrightarrow \qquad \sum_{j=1}^n (p_j - q_j + 1) = 0$$

$$\Rightarrow \quad \sum_{j=1}^n i(p_j - q_j + 1)\alpha = 0 \qquad \Leftrightarrow \qquad \prod_{j=1}^n e^{i(p_j-q_j+1)\alpha} = 1$$

and with Lemma 3.1 it follows

$$\prod_{j=1}^n \tilde{c}_{p_j q_j} = \prod_{j=1}^n e^{i(p_j-q_j+1)\alpha} c_{p_j q_j} = \prod_{j=1}^n c_{p_j q_j}.$$

$\square$